3.6 **EVALUATION OF SMOKE PLUME DISPERSION IN COMPLEX TERRAIN USING A LAGRANGIAN PARTICLE DISPERSION MODEL DRIVEN BY WRF OUTPUT**

Luke Peffers * and Henry Fuelberg
Department of Meteorology, Florida State University

P. Anil Rao
United States Air Force

1. INTRODUCTION

Atmospheric transport and dispersion (T&D) models are used extensively in the research and operational communities. Their applications include forecasting the trajectories of anthropogenic and natural chemical species as well as accidental or intentional releases of hazardous materials. Many T&D models are denoted "offline" because they rely on gridded meteorological data from external numerical atmospheric models to provide the wind and temperature fields used to calculate the trajectories and dispersion of pollutants. Additional parameters are needed to determine the turbulent and mesoscale components of the wind field when the resolution of the gridded meteorological data is insufficient to explicitly resolve these smaller scales of motion.

Given WRF's recent popularity, our study uses it to provide the meteorological data to drive T&D simulations based on the Dabberdt (2004) recommendation to further develop and test the model. WRF is a non-hydrostatic mesoscale model with several options for dynamic cores, as well as various choices for physical parameterizations that allow applications on many different scales (Skamarock 2008).

This type of modeling can be very beneficial, especially in regions of complex terrain and in remote locations such as the Middle East where high-resolution regional forecasts typically are not prepared on a daily basis. Forecasts for AQ and emergency response purposes are highly desirable in such locations, and sensitivity studies investigating the latest advanced numerical modeling capabilities are needed to aid the decision making process of user organizations.

In this study, we explore WRF's fundamental capability as a state-of-the-art atmospheric model to provide the accurate mesoscale representation of the atmosphere that is needed in transport and dispersion applications over highly complex terrain. To isolate WRF as a purely meteorological model, we utilize it in conjunction with an "offline" T&D Model to simulate the transport and dispersion of carbon monoxide (CO) plumes from fires and anthropogenic sources in and near Iran. We use a version of the FLEXPART LPDM that has been adapted to ingest WRF output, hereafter denoted F-W (Fast 2006), to simulate the transport of CO released from fires and anthropogenic sources.

* *Corresponding author address:* Luke Peffers, Florida State Univ., Dept. of Meteorology, Tallahassee, FL 32304;
URL: http://fuelberg.met.fsu.edu/~lpeffers/
Email: lpeffers@met.fsu.edu

We evaluate how various WRF configurations affect simulations of CO plumes in complex terrain. We use F-W model results as the primary measure of effectiveness, while a conventional verification of meteorological conditions against observations provides a secondary measure. Specifically, we present an "effect comparison" of T&D Model simulations that provides the means to document and compare the predominant consequences of particular WRF configurations on the resulting structure and placement of CO plumes. We focus on multiple facets of model physics in non-idealized circumstances to assess their net influence on transport and dispersion. Our study considers configurations involving WRF's 1) horizontal resolution (Test T1), 2) vertical resolution and vertical level configuration (Test T2), 3) planetary boundary layer (PBL) physics (Test T3), and 3) the choice of land surface model (LSM) (Test T4).

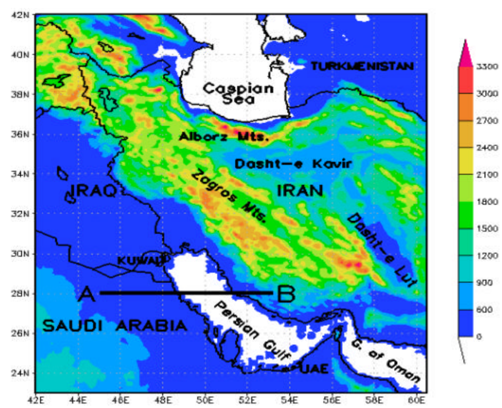

Fig. 1. Geographic map of the AOI. Shading is surface height (m) (8-km resolution).

2. DATA AND METHODOLOGY

2.1 *Study Domain*

We designated an area of interest (AOI) (Fig. 2) in which to perform this evaluation. Our AOI spanned approximately 1,500 × 1,500 km and was centered over central Iran. The dominant orographic features in the AOI are the Elburz and Zagros mountain ranges and the Lut and Salt Deserts (Fig. 1). The three-day period of study was from 22-25 June 2008.

Our baseline WRF computational area (Fig. 2) consisted of an outer domain spanning 5,000 × 5,000 km. The baseline WRF domain included a nested region spanning approximately 2,300 km in the south-north direction and 2,000 km in the west-east direction that encompassed the majority of the AOI. F-W particles representing mass fractions of CO were transported over the sam e 5,000 × 5,000 km area.

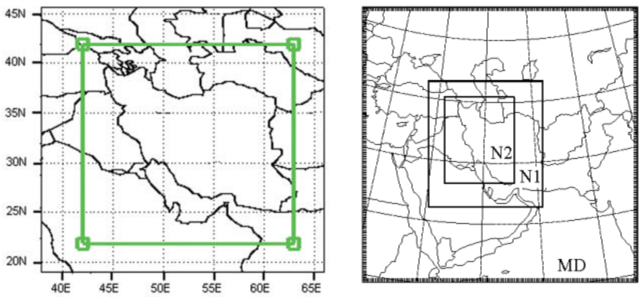

Fig. 2. Boundaries of the AOI (green box in left panel) and WRF domains (right panel). MD is the mother domain (24 km); N1 is the first nest of the baseline configuration (8 km); and N2 is the second nest used for test T5-2 (2.67 km).

2.2 *Meteorological Model*

We performed meteorological simulations to provide input for F-W using version 3.0 of the Advanced Research WRF (ARW) (Skamarock 2008). Damping was employed at the model's top (50 hPa) to prevent reflection from the upper boundary. We initialized WRF's domains and updated the outer domain lateral boundary conditions (LBCs) with GFS Final Analysis data on a 1° × 1° grid at 6-h intervals.

2.3 *Transport Modeling*

a. Transport and dispersion model

We performed transport simulations of CO emissions using the F-W LPDM. A total of 2.2×10^6 particles were released from locations of emissions during the three-day simulations. Mass concentrations within F-W are calculated on a user-defined grid, unlike the particle trajectory calculations. These calculations were made on a 180 × 180 point domain with 28 vertical levels ranging from 0.05 km to 10 km above ground level (AGL). Detailed information on the F-W model is contained in the FLEXPART model documentation (http://zardoz.nilu.no/%7Eandreas/flexpart/flexpart50.pdf).

b. Biomass burning CO emissions

We simulated the CO emissions from observed fires within our WRF outer domain. Their source locations were determined by the Moderate Resolution Imaging Spectroradiometer (MODIS) instrument onboard the Aqua and Terra satellites. These detections use the MOD14 and MYD14 Fire and Thermal Anomalies Products (Justice 2002) to identify 1 km^2 pixels containing fire along with a confidence indicator ranging fom 0 (no confidence) to 100 (full confidence). We included only those fires that were detected with a confidence level of 75 or greater, providing 578 fires during the three-day simulation period (Fig. 3). This choice helps mitigate any positive CO bias that might arise due to false detections. We assumed that each MODIS-detected fire covered a 180 hectare region, similar to Stohl (2007). Since MODIS fire locations are detected during the satellites' overpass, the durations of the fires could not be determined. Therefore, we assumed that any fire detected on a given day burned for 24 h (i.e., 0000 to 2359 UTC). Although an actual fire may not have burned the entire day, it still may have continued to emit CO. In fact, it is estimated that 84% of CO production occurs when a fire smolders (Levine 1991). Our assumption will over predict CO emission from fires that ignited late in the day and were subsequently detected by MODIS. A cause of under predicting CO emission is cloud cover in northern Iran which prevented some MODIS fire detections. However, cloudy conditions were not observed over the majority of Iran from 22-25 June, and the clouds that did occur primarily were located in the northern extent of our AOI (i.e., over and north of the Zagros Mountains). There was no evidence of pyroconvection due to the fires. Thus, we released particles at each fire location in the lowest 100 m of the F-W domain to simulate relatively weak buoyancy due to the fires' release of sensible heat.

We estimated the amount of CO emissions from each detected fire using the equation

$$E = AB\alpha\beta \,, \qquad (1)$$

where A is the area burned, B is the fuel loading (biomass available), α is the fraction of biomass consumed, and β is an emission factor for CO (Stohl 2007). Values of B, α and β were taken from Stohl (2007). To assign the emissions parameters, fire locations were matched with the dominant landuse category in the area.

c. Anthropogenic CO emissions

To achieve the most realistic CO profiles from F-W, we also included CO emissions from anthropogenic sources. We used a global 1° x 1° gridded anthropogenic emissions dataset from the Center of Global and Regional Environmental Research (CGRER) (for further information see http://www.cgrer.uiowa.edu/arctas/emission.html). The primary sources of anthropogenic CO emissions in our AOI were Tehran, Kuwait, Baghdad, Doha, and the UAE (Fig. 3). We only included anthropogenic emissions that exceeded 1.15×10^4 kg (CO) day^{-1} to reduce computational requirements. This accounted for approximately 80% of the total anthropogenic emissions in our F-W domain. The anthropogenic emissions were released in the lowest 100 m.

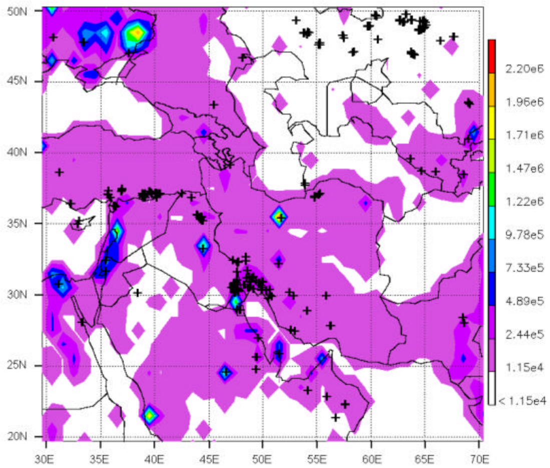

Fig. 3 Emissions sources used in the F-W initialization. MODIS hotspot fire locations (✚) are plotted for fires detected with a confidence of 75 or greater (578 total fires) between 22 - 25 June 2008. Anthropogenic emission estimates are shaded (kg CO day $^{-1}$). Only emissions exceeding 1.15 × 10^{4} kg CO day^{-1} are used in the F-W initialization, accounting for approximately 80% of the total anthropogenic emissions in the domain.

2.4 *Experimental Design*

Four series of sensitivity tests were performed (Table 1). The first sensitivity test evaluated the effect of increasing WRF's horizontal resolution by using two-way nesting over the AOI to better represent the rugged terrain in regions of strong sources of CO emissions (e.g., Kuwait City and Tehran). In the second test we evaluated the effects of various WRF vertical resolutions to better resolve the vertical structure of the PBL. The third sensitivity test evaluated the effects of the different PBL schemes available in the WRF model. These schemes are responsible for vertical fluxes due to unresolved turbulent eddies in the column (Skamarock 2008). The final test evaluated the effect of LSMs that provide the heat and moisture fluxes that are responsible for mechanical mixing in the PBL.

2.5 *Verification*

a. WRF verification

We calculated verification statistics to compare WRF model output to observations within the AOI, as a secondary measure. WRF-derived wind speed, direction, and temperature were compared to observations using conventional verification methods (e.g., RMSE). The observed surface and upper-air winds and temperatures used in the verification were obtained from the National Centers for Environmental Prediction (NCEP).

b. F-W verification

The observed structure of CO concentrations in the AOI was obtained from the Atmospheric Infrared Sounder (AIRS) onboard Aqua, a polar orbiting, sun-synchronous satellite at an altitude of 705 km. The AIRS Level 3 Daily Gridded Product (see http://disc.gsfc.nasa.gov/AIRS/documentation/v4_docs/v4_docs_list.shtml) contains CO retrievals on a 1° × 1° grid at seven pressure levels. We employed an object-based (OB) approach to the forecast and observed 2-D (using total column measurements) CO. The OB approach is part of the Model Evaluation Tools (MET) (http://www.dtcenter.org/met/users/) that was developed by the National Center for Atmospheric Research (NCAR) Developmental Testbed Center (DTC). In addition, heights of smoke plumes were qualitatively diagnosed using cross sections from the Cloud-Aerosol Lidar and Infrared Pathfinder Satellite Observation (CALIPSO) (Vaughan 2004). Quantitative evaluation using CALIPSO data could not be performed because the aerosol retrievals were dominated by sand which obscured the smoke signal. However, the CALIPSO Vertical Feature Mask (VFM) product does discriminate between sand and polluted sand (a combination of sand and biomass burning smoke).

Table 1. Sensitivity tests performed in the study

Baseline :	One nest @ 8 km resolution 40 vert. levs., YSU PBL, and 5-Lay. LSM
<u>Test T1–Horizontal resolution</u>	
T1-1:	Two nests @ 8 and 2.67 km resolution
T1-2:	Two nests @ 8 and 1.6 km resolution
<u>Test T2–Vertical resolution</u>	
T2-1:	50 vert. levs evenly spaced
T2-2:	50 vert. levs. packed in PBL
T2-3:	50 vert. levs. packed in mid trop.
T2-4:	50 vert. levs. packed in upper trop.
<u>Test T3–Planetary boundary Schemes</u>	
T3-1:	MYJ PBL
T3-2:	ACM2 PBL
<u>Test T4–Land surface models</u>	
T4-1:	Noah LSM
T4-2:	RUC LSM
T4-3:	Pleim-Xiu LSM

3. RESULTS

This section describes the fields of CO concentration that were produced by our various T&D simulations. We analyze total column and vertical profiles of CO to identify significant plumes for further study (actually large areas of high concentration consisting of several smaller-scale plumes).

3.1 *Modeled Plume Structure*

Figure 4 shows two prominent CO plumes in the AOI during the baseline run. Plume 1 of the baseline simulation (hereafter denoted BP1) forms over northeastern Saudi Arabia and Kuwait, and extends over the northern portion of the Persian Gulf (Fig. 4). BP1 is due to a shortwave trough that develops over north central Saudi Arabia and then propagates to southern Kuwait on 23-24 June. Vertical cross sections through BP1 (Figs. 5 and 6 at two times 12 h apart show that the overall plume consists of several components of high concentration. Greatest CO concentrations (i.e., exceeding 45 μg m^{-3}) during the daytime are located between 2 and 4 km AGL and also near 1 km in the region of the land-sea circulation. At night (Fig. 6), greatest CO concentrations are found near ground level.

The altitude of the PBL changes greatly along the cross sections. The daytime PBL over the desert region west of Iran exceeds 4 km AGL due to surface heating, but then subsides to near-ground level at night as the surface cools and mixing subsides. Conversely, the marine PBL generally remains very near the surface during both day and night as depicted by the steep PBL gradient near the coastline. The vertical extent of the pollutants in these cross sections (~ 5 km AGL) approximately represents the level of the residual mixed layer above the nighttime PBL.

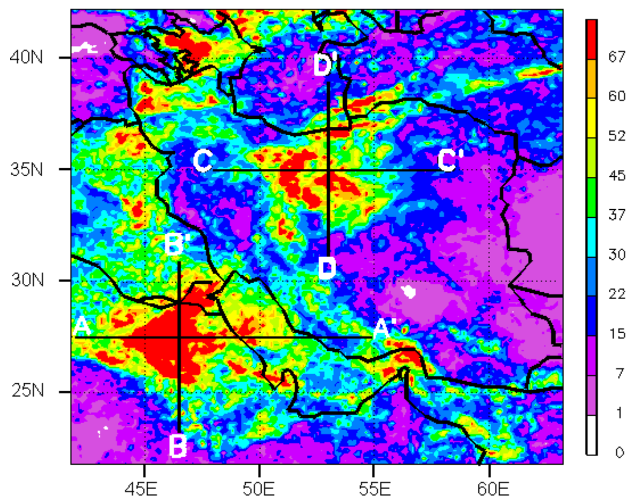

Fig. 4. Baseline 72 h simulation of total column CO (mg m^{-2}) in the AOI. White ovals indicate locations of the two plumes. Plume BP1 is located near 27°N, while plume BP2 is located farther north at approximately 35°N. Locations of cross section through the plumes are indicated by black lines. Lines from A to A' and B to B' are for the cross sections in Figs. 10 and 11. Lines from C to C' and D to D' are for cross sections in Figs. 12 and 13.

Baseline Plume 2 (hereafter denoted BP2) begins over northern Iran and extends to Turkmenistan and the southern portion of the Caspian Sea (Fig. 4). It also consists of several components but is less defined than BP1. BP2 apparently forms because of weak PBL ventilation (i.e., the product of PBL height and the mean wind speed within the PBL) that prohibits pollutants from being transported out of the region. Cross sections of BP2 (Figs. 7 and 8) show that greatest concentrations exceeding 45 µg m^{-3} are located between 2 and 6 km AGL during both day and night. The daytime PBL over central Iran exceeds 3000 m AGL (Fig. 7), but at night subsides to only tens of meters (Fig. 8). There is significant spatial variability near the transition from the mountains in northern Iran to the Caspian Sea in the north (Fig. 7)

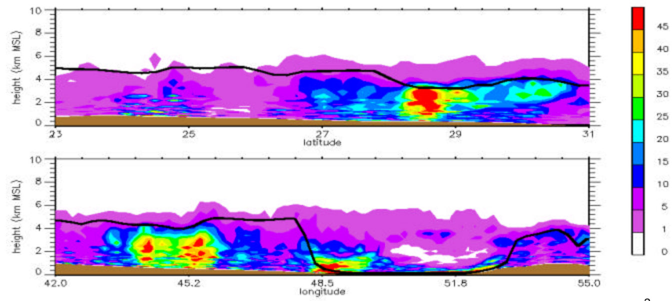

Fig. 5. Cross section of CO concentration by volume (µg m^{-3}) through BP1 from B to B' (top panel) and from A to A' (bottom panel) in Fig. 9 at 12 UTC 24 June. The thick black line represents the top of the PBL

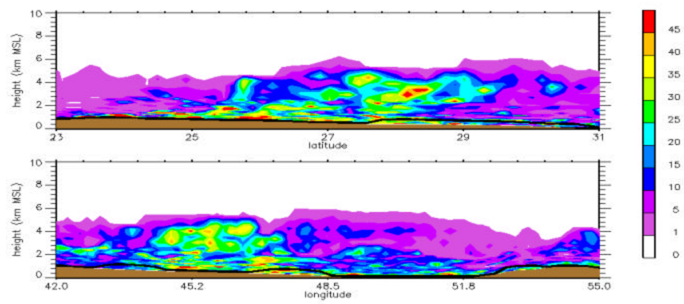

Fig. 6. As in Fig. 5, but at 00 UTC 25 June.

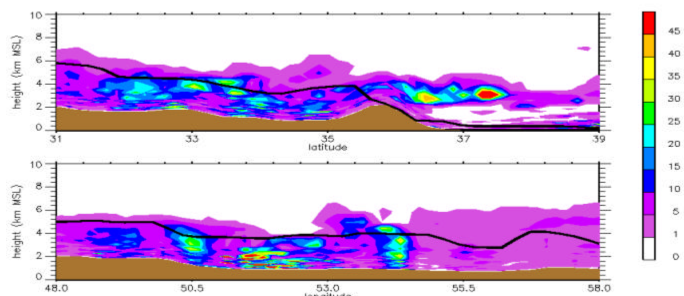

Fig. 7. Cross section of CO concentration by volume (µg m^{-3}) through BP2 from D to D' (top panel) and from C to C' (bottom panel) in Fig. 9 at 12 UTC 24 June. The thick black line represents the top of the PBL.

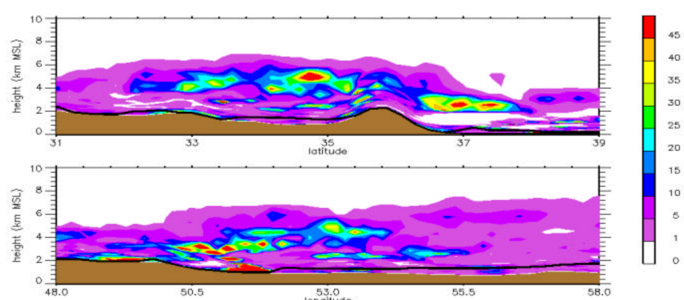

Fig. 8. As in Fig. 7 but at 00 UTC 25 June.

Small structural differences in the plumes (not shown) were observed in the various tests involving WRF's horizontal and vertical resolution (tests T1 and T2 respectively). The tests investigating different PBL schemes and LSMs (tests T3 and T4 respectively) produced large structural differences in both plumes in all three spatial dimensions due to differences in PBL heights that were as great as 1500 m (not shown). The large plume variability produced by the various LSMs was due to differences in surface sensible heat fluxes as great as 500 W m^{-2} (not shown).

3.3 *Model Verification*

a. Meteorological simulations

Due to the limited amount of radiosonde data (i.e., < 10 sites) within the AOI, most of the changes in ME are not statistically significant at the 90% CI. Furthermore, despite the relatively large number of surface observations (i.e., > 300 within the AOI) many changes in the RMSEs of the various simulations also are not significant. Thus, we only briefly discuss the most significant findings.

The results indicate a general improvement in the accuracy of wind speed and direction when increasing WRF's horizontal and, to a lesser extent, its vertical resolution, especially when more vertical levels were packed in the PBL. However, contrary to what one might expect, the results from T1-2 suggest that increasing the horizontal resolution to 1.6 km does not add more skill than the simulation using 2.67 km resolution. This can be the effect of inconsistent vertical and horizontal resolutions and/or the result of a larger course-to-fine grid nesting ratio (i.e., 1:5 vs. 1:3). Results also show that the various PBL schemes and LSMs produced the most significant changes in the meteorological parameters with no clear superior scheme.

b. Transport simulation--Comparison with AIRS

We next compare the two simulated plumes to remotely sensed CO retrievals from the AIRS sensor onboard the Terra polar-orbiting satellite. Terra passed over the Middle East at approximately 2230 UTC 24 June, providing nearly continuous CO retrievals over the AOI (Fig. 9). AIRS retrievals contain little information about the vertical distribution of CO since only approximately two independent levels of information are available (see http://disc.gsfc.nasa.gov/AIRS/documentation/v4_docs/v4_docs_list.shtml). Nonetheless, the AIRS verticality product (Fig. 10) indicates significant low level (i.e., below 800 hPa) CO concentrations in the AOI, and this layer appears to be the primary contributor to the observed pattern in Fig. 9. AIRS verticality is a measure of sensitivity, indicating the amount of information that is retained from the base state (first guess) CO profile (i.e., 1 minus the values in Fig. 10 equals the amount of information retained from the base state profile) (McMillan 2005).

Comparisons between AIRS total column CO and CO from the baseline T&D simulations reveal several major inconsistencies. For example, the AIRS retrievals indicate a large CO maximum over the Caspian Sea that is not captured by the baseline (Fig. 9). Backward trajectories from this plume (not shown) reveal that it originated over the eastern Ukraine and then moved toward northern Iran. However, tracer particles cannot be transported such a long distance during the relatively short duration of our simulations. Therefore, we will not compare data in the region of this plume even though it partially lies within the AOI.

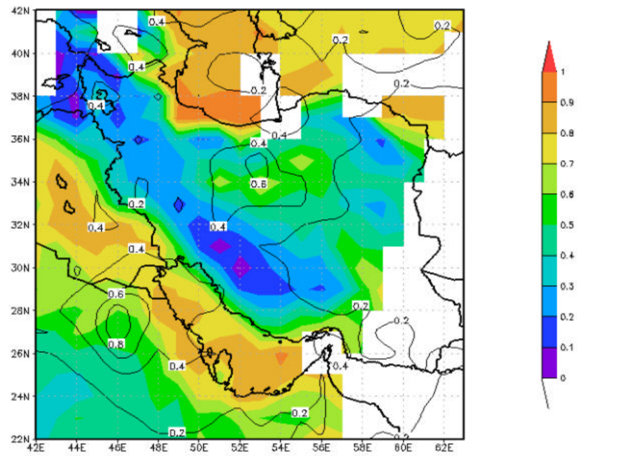

Fig. 9 Normalized total column CO from AIRS (shaded) and from the baseline simulation (contoured).

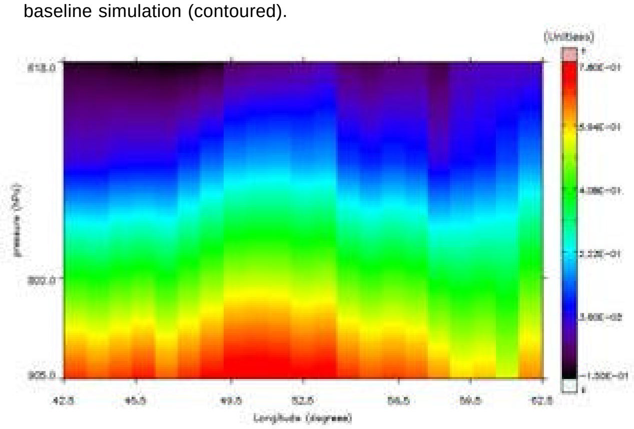

Fig. 10. AIRS CO verticality averaged between 22–42^{o}N at 2330 UTC 24 June. One minus these values indicates the amount of information retained from the basic state CO profile.

Another notable difference is between BP1 and the AIRS CO maximum over the Persian Gulf (denoted OP1) (Fig. 9). Specifically, OP1 is much more diffuse than BP1, primarily over the open water. Although this observation may be biased by AIRS' tendency to slightly overestimate CO concentrations over oceans (Warner 2007), OP1's structure is not unreasonable since it is oriented along the strong northwesterly winds downwind of large emission sources in Kuwait and Iraq. Since this inconsistency appears to reflect a limitation in the T&D simulation, this plume will be included in the object based verification that follows

Inconsistencies between the AIRS and the baseline simulations of BP2 (Fig. 9) appear to be due to modeling difficulties associated with the complex terrain within the AOI. Therefore, we will present comparative analyses that quantify these differences for each simulation using MET's OB verification approach. These statistical scores will indicate changes in performance that result from the various WRF configurations.

Figure 11a shows the results of verifying OB1 with Plume 1 as simulated by each test series. The bars indicate each simulation's skill (in terms of CSI) at reproducing CO "objects" that resemble AIRS' observed "objects". The forecast and observed "objects" were defined by applying a threshold (= 0.52) to the normalized AIRS and F-W data in MET's OB tool. The skill score of the baseline simulation is indicated by the far left bar of the graph so it can easily be compared to those of the simulations.

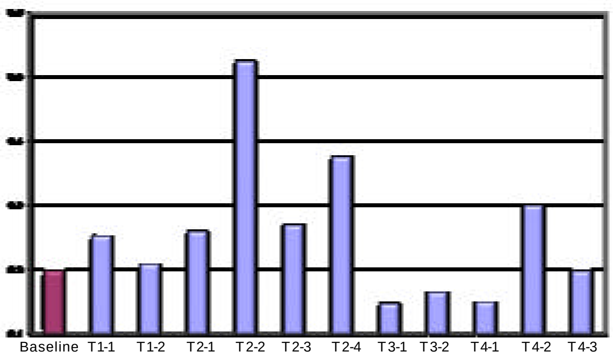

a)

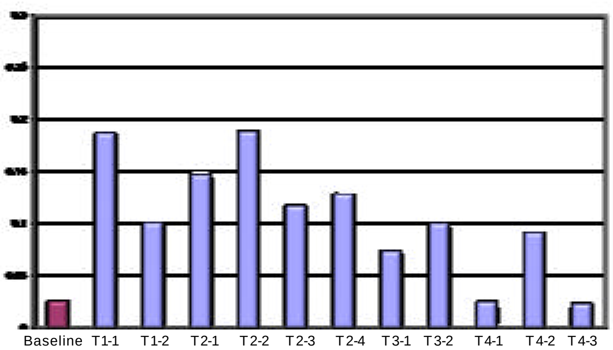

b)

Fig. 11. CSI scores from the MET OB verification of Plume 1 (upper panel) and Plume 2 (lower panel). The red bar indicates the CSI of the baseline simulation. Blue bars indicate the CSI for the test series as labeled.

Figure 11a shows that all of the T1 and T2 series outperform the baseline in their ability to match the pattern of OB1. Thus, increasing either WRF's horizontal or vertical resolution leads to improved skill in matching OB1. Similar to the meteorological verification results, increasing the horizontal resolution to 1.6 km does not increase the accuracy of the simulation beyond what is achieved at 2.67 km resolution. The best match is produced by T2-2 in which WRF's vertical levels are packed near the surface. T2-4's ability to match OB1 also is far superior to the baseline, indicating that packing the vertical levels in the upper levels adds skill. Compared to the T1 and T2 tests, the T3 and T4 series do not produce improved skill. Only T4-2 outperforms the baseline. Thus, only the RUC LSM scheme adds skill in simulating the Arabian Desert and Persian Gulf areas, whereas the MYJ PBL, ACM2 PBL, Noah LSM schemes degrade the simulation.

Figure 11b shows results of verifying OB2 with Plume 2 using the same threshold as before. The baseline simulation poorly matches the features of OB2, as indicated by the small overall CSI score (< 0.2) for all simulations. The smaller CSI scores compared to those observed in Fig. 11a are due to the segmented nature of Plume 2. That is, the OB verification process defines a greater number of relatively small objects, providing a greater opportunity for misses and false alarms. Once again, T1 and T2 produce the largest CSI compared to the baseline, with T2-2 superior to all other test series. The skill of T1-1 is similar to that of T2-2, showing that increased horizontal resolution (up to 2.67 km) improves forecast skill nearly as much as increasing the vertical resolution in the PBL. Two of the three simulations comprising the T4 series match OB2 as well as the baseline, whereas T4-2 (i.e., RUC LSM) produces a better match than the baseline. The two T3 simulations considerably outperform the baseline. Thus, increased horizontal and vertical resolution adds forecast skill in Iran's mountainous interior. The MYJ PBL, ACM2 PBL, and RUC LSM schemes also improve simulation skill in matching OB2, whereas the Noah and Pleim-Xiu LSM schemes do not significantly affect the skill.

The results of OB2 are similar to those of OB1 with two notable exceptions: First, the MYJ and ACM2 PBL schemes both produce smaller CSI scores for OB1 than the baseline. This further suggests that the low PBL heights compared to the baseline are inaccurate, especially over the Arabian Desert. Second, increasing the vertical resolution over the Arabian Desert is most affected when the added levels are confined to lower altitudes, whereas over Iran's mountainous terrain, increasing the vertical levels at all altitudes adds significant skill. This can be explained by examining the vertical level configurations. Due to the nature of WRF's terrain following vertical coordinate, the vertical levels become more horizontal as one approaches the model top (i.e., 50 hPa). Thus, the vertical levels are more tightly packed in the lower troposphere when topography is introduced. This has the effect of increasing the vertical resolution in the lower troposphere in areas of mountainous terrain. Therefore, the model is less sensitive to the altitude at which the vertical resolution is increased over Iran's mountains since the resolution already is slightly higher.

c. Transport simulation--comparison with CALIPSO

The CALIPSO sensor passed over the AOI at approximately 2230 UTC 24 June. Therefore, our simulated biomass burning only CO plumes (anthropogenic sources turned off) can be compared to CALIPSO's aerosol profiles if we assume that the fires release large quantities of CO which follow the trajectories of the associated aerosols. We compared CALIPSO's aerosol vertical feature mask data (Vaughan 2004) (Fig. 12) to cross sections of simulated CO on the final day of the simulation, i.e., 2230 UTC 25 June. This time was chosen so the simulated plumes could mature from the initial "zero CO domain". The CALIPSO data are sensitive to cloud cover, and clouds can even cause a total attenuation of the LIDAR beam, producing a data void below cloud level. Because convective clouds were present in and north of Iran, data voids are observed, especially north of the Alborz Mountains (red circle in Fig. 12).

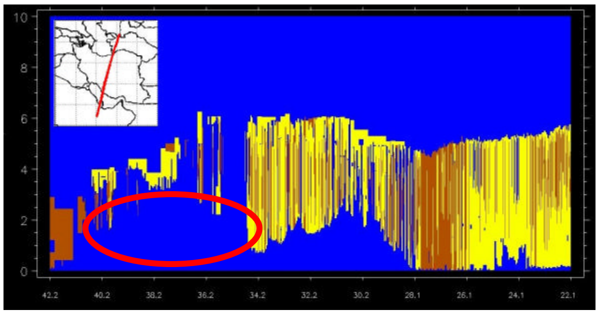

Fig. 12. CALIPSO Vertical Feature Mask at approximately 2230 UTC 24 June within the AOI. Yellow indicates sand aerosols, and brown indicates polluted sand (i.e., a mixture of sand and biomass burning aerosols). The red oval indicates total attenuation of CALIPSO's beam by cloud cover. One should note that the chart represents CALIPSO's true ground track (on its descending node); thus latitude *decreases* along the abscissa from left to right.

The biomass burning only CO cross section from the baseline simulation that corresponds to CALIPSO's ground path is presented in Fig. 13. CALIPSO's path intersects both Plumes 1 and 2, providing an observed vertical profile of each. It is encouraging that locations along CALIPSO's path that are categorized as polluted sand (i.e., sand and biomass burning smoke aerosols) correspond to regions of enhanced CO in the baseline cross section. Specifically, the tall column of CALIPSO-detected smoke aerosol over the Persian Gulf (between ~28-26°E) corresponds to large simulated concentrations in that area. Additional agreement is seen over Iran's mountainous interior, and elevated concentrations of simulated CO near 23°N correspond well with CALIPSO's aerosol pattern. However, large concentrations exceeding 10 µg m^{-3} at ~5 km above sea level (ASL) appear to represent an over prediction based CALIPSO's relatively weak signal of smoke aerosol compared to the signal depicted over the Persian Gulf. Finally, the depth of the assumed residual layer (between ~ 4– 6 km ASL) in CALIPSO's VFM agrees well with that of the baseline simulation.

It is difficult to quantify each simulation in terms of its ability to match CALIPSO's VFM because the smoke classification estimates are not adequate to resolve individual plumes. Therefore, we qualitatively selected one simulation from each test series that appears to best match the pattern seen in Fig. 12. Vertical cross sections of the simulations determined to best match CALIPSO's aerosol product are presented in Figs. 30-33.

T1-1 appears to replicate the pattern of airborne aerosols depicted by CALIPSO's aerosol product (Fig. 14), whereas T1-2 depicts larger surface concentrations over the Persian Gulf. T2-2 provides the best match of its series, especially in the region of Plume 1 (i.e., the elevated concentrations between 26-28°N (Fig. 15). The other T2 simulations produce maximum concentrations at those latitudes that either are much too near the surface or are displaced horizontally. T3-2 (ACM2 PBL scheme) also replicates rather well the elevated CO concentrations in the region of Plume 1, but appears to over predict near-surface CO concentrations (Fig. 16). Elevated concentrations from T3-2 at ~ 2 – 5 km ASL in the region of Plume 2 (i.e., near 34°N) also resemble the aerosol profile in Fig. 12; however, T3-2 appears to slightly over predict the altitude of CO over the Caspian Sea between ~ 39-40°N. T4-3 (Pleim-Xiu LSM) (Fig. 17) is the best match of the T4 series; however, it appears to produce, perhaps erroneously, large elevated concentrations over Iran's interior that are similar to the baseline. T4-3 also appears to overestimate the depth of the residual layer near 32°N -32°N by ~ 1 km. Similar to T3-2, T4-3 also appears to over predict the altitude of CO over the Caspian Sea.

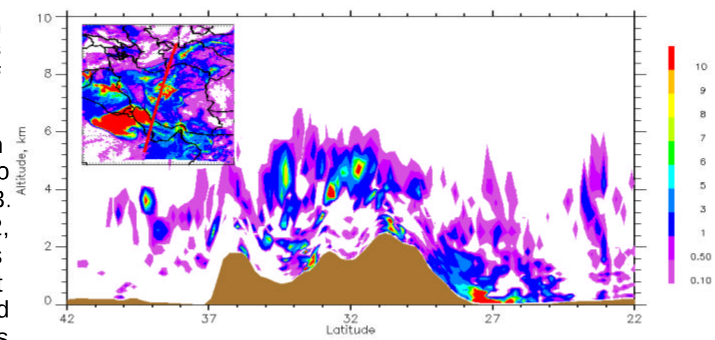

Fig. 13. Vertical cross section of simulated CO (µg m^{-3}) from the baseline simulation corresponding to the CALIPSO cross section in Fig. 12. The inset panel is the total column CO that is contributed only by biomass burning. The red line in the inset indicates CALIPSO's ground track and the location of the cross section. Plumes One and Two are represented in this cross section as seen in the inset plot of total-column CO from biomass burning. The eastern portion of Plume One is seen at about 27°N, while portions of Plume 2 are seen between 30-35°N. The figure represents CALIPSO's true ground track; thus latitude *decreases* along the abscissa from left to right.

The results discussed above provide further evidence that increasing WRF's horizontal and vertical resolution, especially at lower altitudes produces more accurate T&D simulations. It is also seen that the 2.67 km resolution simulation outperformed the 1.6 km resolution simulation similar to the previous verification results. Results from the T3 series provide further evidence that the ACM2 PBL scheme outperforms the MYJ PBL scheme, whereas it appears to resemble the plume structure produced by the baseline (i.e., YSU PBL). Finally, the T4 results indicate that the Pleim-Xiu LSM provides more accurate T&D simulation than the RUC and Noah LSMs, but less accurate than the baseline (i.e., 5-Layer thermal diffusion LSM).

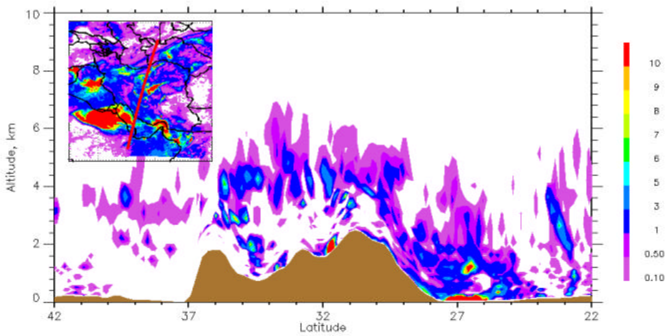

Fig. 14. As in Fig 13, but for the T1-1 simulation (i.e., 2.67 km horizontal resolution).

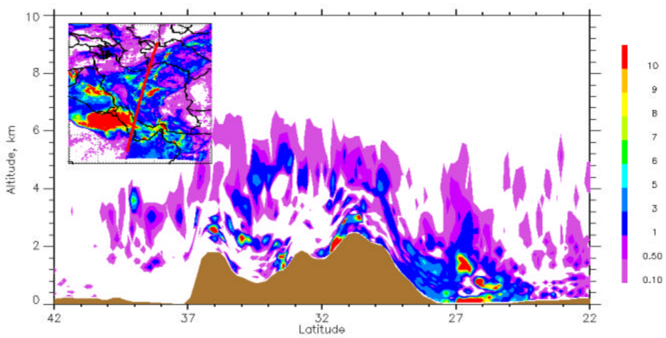

Fig. 15. As in Fig 13, but for the T2-2 simulation (i.e., 50 vertical levels packed in the PBL).

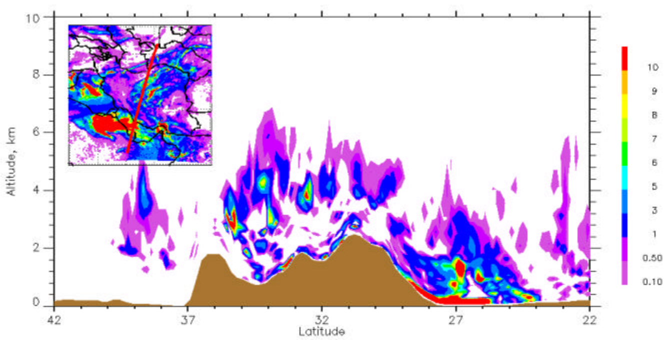

Fig. 16. As in Fig. 13, but for the T3-2 simulation (i.e., the ACM2 PBL scheme).

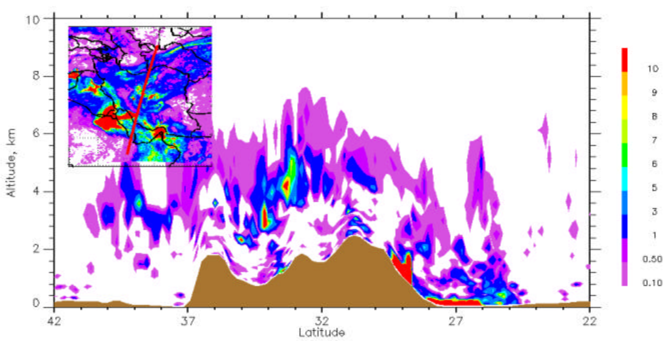

Fig. 17. As in Fig. 13, but for the T4-3 simulation (i.e., the Pleim-Xiu LSM model).

4. SUMMARY AND CONCLUSIONS

The study utilized the FLEXPART Lagrangian Particle Dispersion Model (LPDM) (Stohl 2005) that was adapted to ingest WRF output (denoted F-W) at hourly intervals. We performed four series of simulations over Iran and surrounding regions. The tests were designed to document T&D model sensitivities to WRF's 1) horizontal resolution (Test T1), 2) vertical resolution and vertical level configuration (Test T2), 3) planetary boundary layer (PBL) physics (Test T3), and 3) the choice of land surface model (LSM) (Test T4).

Results showed that increasing WRF's horizontal resolution from 8 km to 2.67 km and then to 1.6 km primarily altered the horizontal structure of the Iranian plume, whereas the Arabian Desert plume was only slightly affected. Furthermore, increasing the vertical resolution from 40 to 50 levels and packing the levels either in the PBL, mid troposphere, or the mid-to-upper troposphere only produced slight changes in the plumes' structure. Conversely, tests investigating different PBL schemes and LSMs produced large structural differences in both plumes in all three spatial dimensions due to differences in PBL heights that were as great as 1500 m. The large plume variability produced by the various LSMs was due to differences in surface sensible heat fluxes as great as 500 W m^{-2}. These large differences in sensible heat flux may be a response to the LSMs' treatment of soil moisture data that were used to initialize the model. Recent studies have shown that large errors can occur if a LSM utilizes poor quality soil moisture data to initialize the meteorological model. For example, Pleim and Xiu (2003) stated that inadequate initial soil moisture conditions can be detrimental to air quality (AQ) forecasts since they can severely affect the evolution of the PBL.

It was important to determine whether the abovementioned differences in WRF output affected the accuracy of the T&D simulations. Therefore, we compared our simulated results to observations. Satellite-derived plume data were used to quantitatively verify our simulated CO plumes against the AIRS total-column CO data using an object-based approach (OB). OB verification techniques have been used in recent studies of meteorological parameters such as precipitation (e.g., Davis 2006; Wernli 2008) and reflectivity (e.g., Marzban 2008). However, to our knowledge no studies have utilized an OB approach to verify simulated CO plumes against satellite-derived plumes. We also presented traditional verification statistics (i.e., RMSE) that compared WRF-derived winds and temperatures to observations. However, we consider our verification of the meteorological parameters to be a secondary source of information because it does not consider the CO plumes directly. Finally, the vertical structure of CO plumes produced by fires was qualitatively compared to CALIPSO's satellite-derived aerosol data by assuming that airborne aerosols approximately follow the trajectories of CO emitted by the fires. We observed few statistically significant differences (at the 90% confidence interval) when comparing the various simulated winds and temperatures with observations. However, the results did indicate a general improvement in the accuracy of wind speed and direction when increasing WRF's horizontal and, to a lesser extent, its vertical resolution, especially when more vertical levels were packed in the PBL. However, contrary to what one might expect, the results from T1-2 suggested that increasing the horizontal resolution to 1.6 km does not add more skill than the simulation using 2.67 km resolution. This can be the effect of inconsistent vertical and horizontal resolutions and/or the result of a larger course-to-fine grid nesting ratio (i.e., 1:5 vs. 1:3). Results also showed that the various PBL schemes and LSMs produced the most significant changes in the meteorological parameters.

The OB comparisons of plume structure (i.e., total-column CO) revealed marked changes in the ability of the T&D simulations to replicate the two primary plumes. Results for the Arabian plume showed that F-W's ability to replicate it was considerably enhanced by increasing WRF's horizontal and vertical resolution. However, the simulation with 2.67 km resolution produced a better match than the 1.6 km simulation, similar to the results from the meteorological verification. The greatest improvements occurred when the vertical resolution was increased, especially in the PBL. Results from WRF's various PBL options showed that the MYJ and ACM2 schemes' anomalously low PBL heights in the desert regions degraded the simulations' ability to replicate the Arabian Desert CO plume. Only the RUC LSM increased the verification score due to its more realistic surface sensible heat fluxes compared to the other LSMs. The Pleim-Xiu LSM matched the Arabian plume with similar accuracy as the baseline, whereas the Noah LSM degraded the simulation accuracy.

Verification results for the Iranian plume were similar to those of the Arabian Plume, but with generally lower CSI scores. Increased horizontal resolution was found to improve the verification score nearly as much as increasing the vertical resolution in the PBL. Again, the 2.67 km simulation outperformed the 1.6 km simulation. The increased vertical resolution over the mountains was found to be less sensitive to the altitude of the enhanced resolution than over the deserts. Contrasting with the Arabian plume, the various PBL simulations produced significantly better CSI scores for the Iranian plume than the baseline. The simulations involving the various LSMs generally produced CSI scores that were very close to those of the baseline; the exception was RUC LSM which outperformed the baseline.

Finally, we extended the verification process to qualitatively consider the vertical profiles of the plumes. We used CALIPSO's space based aerosol classification product to evaluate along CALIPSO's ground track the simulated CO plumes that were due only to biomass burning. The qualitative analysis indicated that the baseline simulation's vertical CO profile agreed well with CALIPSO's aerosol Vertical Feature Mask (VFM) product. Specifically, the height of the residual layer in CALIPSO's aerosol product (ranging from ~ 4 - 6 km) corresponded well with the simulated results. Simulated areas of elevated high CO concentration also coincided with those of enhanced aerosols along CALIPSO's ground track, although the simulations may have over predicted the concentrations in the region of the Iranian plume.

Increasing WRF's horizontal resolution to 2.67 km and then to 1.6 km was found to increase F-W's ability to replicate the vertical profile of airborne pollutants. However, the 2.67 km simulation produced the best match, similar to previous results. Furthermore, increasing the vertical resolution in the PBL provided the best match of the vertical level test series, especially in the region of the Arabian Desert and Persian Gulf. Likewise, simulations using the ACM2 PBL and Pleim-Xiu LSM appeared to provide the best matches of this test series. Although these simulations performed best of the T3 and T4 series, their performance was not improved as much as the T1 and T2 series. The ACM2 PBL simulation better replicated the elevated high concentrations of CO over the Arabian Desert and Persian Gulf than the other PBL simulations and all of the LSM simulations.

Current results show how sensitive the T&D simulations are to choices in configuring WRF, and which configuration parameters yield the best results over complex terrain. Although OB methods previously have not been used to consider satellite-derived plume structures, this study suggests that the method can identify improvements in simulation accuracy. That is, current OB verification results, together with traditional verification statistics, suggest that increasing horizontal resolution beyond 8 km and increasing vertical resolution especially at low altitudes produce significantly more accurate T&D simulations. The results also highlight the large sensitivity of T&D processes to the choice of the PBL scheme, LSM and, perhaps soil moisture initialization data. Future work will seek to exploit this new verification capability to further understand the sensitivities of AQ forecasting.

REFERENCES

Dabberdt, W.F., M.A. Carroll, D. Baumgardner, G. Carmichael, R. Cohen, T. Dye, J. Ellis, G. Grell, S. Grimmond, S. Hanna, J. Irwin, B. Lamb, S. Madronich, J. McQueen, J. Meagher, T. Odman, J. Pleim, HP. Schmid, and D.L. Westphal, 2004: Meteorological Research Needs for Improved Air Quality Forecasting: Report of the 11th Prospectus Development Team of the U.S. Weather Research Program*. *Bull. Amer. Meteor. Soc.*, **85**, 563–586.

Davis, C., B. Brown, and R. Bullock, 2006: Object-Based Verification of Precipitation Forecasts. Part I: Methodology and Application to Mesoscale Rain Areas. *Mon. Wea. Rev.*, **134**, 1772–1784.

Davis, C., B. Brown, and R. Bullock, 2006: Object-Based Verification of Precipitation Forecasts. Part II: Application to Convective Rain Systems. *Mon. Wea. Rev.*, **134**, 1785–1795.

Developmental Testbed Center, 2008: MET: Version 1.1 Model Evaluation Tools User's Guide. [Available onlineat http://www.dtcenter.org/met/users/docs/overview.php. 168 pp.].

Fast, J. D., Easter, R. C., 2006: A Lagrangian Particle Dispersion Model Compatible with WRF. *7th WRF User's Workshop*, Boulder, CO, P6.2.

Justice C. O., J. R. G. Townshend, E. F. Vermote, E. Masuoka, R. E. Wolfe, N. Saleous, D. P. Roy, and J. T. Morisette, 2002: An overview of MODIS land data processing and product status. *Remote Sens. Environ.*, **83**, 3–15.

Levine, J. S., Ed., 1991: *Global Biomass Burning.* The MIT Press, 569 pp

Marzban, C., S. Sandgathe, and H. Lyons, 2008: An Object-Oriented Verification of Three NWP Model Formulations via Cluster Analysis: An Objective and a Subjective Analysis. *Mon. Wea. Rev.*, **136**, 3392–3407.

McMillan, W. W., and Coauthors, 2005: Daily global maps of carbon monoxide from NASA's Atmospheric Infrared Sounder. *Geophys. Res. Lett.,* **32,** L11801, doi:10.1029/2004GL021821.

Pleim, J.E., and A. Xiu, 2003: Development of a Land Surface Model. Part II: Data Assimilation. *J. Appl. Meteor.*, **42**, 1811–1822.

Skamarock W. C., J. B. Klemp, J. Dudhia, D. O. Gill, D. M. Baker, M. G. Duda, X. Huang, W. Wang, and J. G. Powers, 2008: A description of the Advanced Research WRF version 3. NCAR Tech. Note NCAR/TN-475+STR, 113 pp.

Stohl A., C. Forster, A. Frank, P. Seibert, and G. Wotawa,2005: Technical Note: The Lagrangian particle dispersion model FLEXPART version 6.2. *Atmos. Chem. Phys. Discuss*., **5**. 4739-4799.

______, Forster C., Huntrieser H., Mannstein H., McMillan W. W., Petzold A., Schlager H., and Weinzierl B, 2007: Arctic smoke – record high air pollution levels in the European Arctic due to agricultural fires in Eastern Europe, *Atmos. Chem. Phys. Discuss*, **7**, 913-937

Vaughan M., S. Young, D. Winker, K. Powwell, A. Omar, Z. Liu, Y. Hu, and C. Hostetler, 2004: Fully automated analysis of space-based lidar data: An overview of the CALIPSO retrieval algorithms and data products. *Laser Radar Techniques for Atmospheric Sensing,* U. N. Singh, Ed., International Society for Optical Engineering (SPIE Proceedings, Vol. 5575), 16–30.

Warner, J. X., M. McCourt Comer, C. Barnet, W. W. McMillan, W. Wolf, E. Maddy, G. Sachse, 2007: A Comparison of Satellite Tropospheric Carbon Monoxide Measurements from AIRS and MOPITT During INTEX-NA, *J. Geophys. Res*., doi:10.1029/2006JD007925.

Wernli, H., M. Paulat, M. Hagen, and C. Frei, 2008: SAL—A Novel Quality Measure for the Verification of Quantitative Precipitation Forecasts. *Mon. Wea. Rev.*, **136**, 4470–4487.